IBIC characterization of charge transport in CdTe : Cl

© P.J. Sellin¶, A.W. Davies, F. Boroumand, A. Lohstroh, M.E. Özsan, J. Parkin, M. Veale

Department of Physics, University of Surrey,
Guildford GU2 7XH, UK

(Получена 12 сентября 2006 г. Принята к печати 3 октября 2006 г.)

Studies of charge transport uniformity in bulk CdTe : Cl have been carried out using ion beam induced charge (IBIC) imaging. High resolution maps of charge collection efficiency, mobility-lifetime product ($\mu\tau$) and drift mobility (μ) were measured using a scanning microbeam of 2 MeV protons focused to a beam diameter of $\sim 3\,\mu$m. Excellent charge transport uniformity was observed in single crystal CdTe : Cl, with electron $\mu\tau$ values of up to $5 \cdot 10^{-3}$ cm^2/Vs. The presence of extended defects such as tellurium inclusions was also studied using IBIC, and their influence on the charge transport performance of CdTe detector structures is discussed.

PACS: 72.80.Jc, 79.20.Rf, 61.80.Jh

1. Introduction

The development of the high-Z compound semiconductors CdTe and CdZnTe has been studied for many years for use as ionizing radiation detectors. Most recently there has been sustained progress in the development of high quality semi-insulating (SI) CdTe and CdZnTe material of the type required for high efficiency X-ray and gamma ray sensors, due to both improvements in crystal growth technology and to improved understanding of material properties. This activity comes at a time when there is renewed interest in room temperature X-ray and gamma ray detectors for a range of applicants, including medical imaging, homeland security, synchrotron applications, and space science [1–3].

In this paper we describe characterisation measurements of the charge transport properties of single crystal CdTe : Cl using ion beam induced charge (IBIC) imaging. The IBIC technique combines the high spatial resolution of microfocussed MeV ion beams (with a typical spot size of $1-3\,\mu$m) with a very low charge injection regime. By measuring the induced pulse due to the interaction of a single ion in the material, parameters such as carrier drift length, drift mobility and lifetime can be measured in a mapping mode. By restricting the beam fluence to < 1 kHz the time-averaged charge generation rate is ~ 50 pA, so avoiding problems associated with space charge limited currents which can occur in other CD beam injection techniques such as EBIC.

IBIC is a particularly powerful tool to investigate the uniformity of charge transport in bulk semiconductors, and the influence of extended features such as grain boundaries, precipitates and twins on charge transport [4]. In both CdTe and CdZnTe the presence of tellurium inclusions is well known and have been observed, for example, in both undoped CdTe and in high resistivity compensated materials such as the CdTe : Cl used in this study. The presence of high densities of tellurium inclusions has been shown to reduce the resistivity of SI material [5]. In the highest quality CdTe : Cl material grown by the traveling heater method (THM) the density of inclusions in the centre of the crystal can be extremely small, however the exact density and average size of Te inclusions is found to depend sensitively on the exact growth conditions. Various studies have been made to anneal as-grown CdTe wafers in an attempt to reduce the size of the inclusions, and in THM material a significant reduction in inclusion size has been achieved by annealing in argon at temperatures up to 850°C [6].

Other groups have applied various optical techniques to study tellurium inclusions, such as cathodoluminescense (CL) and Raman scattering [7]. Studies using a focused alpha particle radioisotope source have also demonstrated correlations in CdZnTe between tellurium inclusions and spectroscopic performance with limited spatial resolution [8].

The IBIC technique used in this study was initially developed at the University of Surrey for studies of charge transport uniformity in CVD diamond. In this work we report the use of IBIC for mapping of charge collection efficiency and carrier drift length in CdTe, and also in a time resolved mode for studies of carrier lifetime and mobility mapping.

2. Theory

The conventional mode for the IBIC technique is to measure charge signal amplitude, which is directly proportional to carrier drift length λ. The carrier drift length is the fundamental material property which controls the charge collection efficiency (CCE) of a semiconductor detector. In high purity semiconductor materials electron and hole drift lengths are large, and much greater than the active depth of the device, and devices generally exhibit 100% CCE.

In CdTe and CdZnTe trapping effects tend to limit the carrier drift lengths, and hence the CCE. In general for a detector of thickness d, the CCE ε can be expressed by

$$\varepsilon = \frac{Q}{Q_0} \approx \frac{qN_0}{d}\,(\lambda_e + \lambda_h), \qquad (1)$$

where λ_e and λ_h are the mean drift lengths for electrons and holes, respectively. For nonsaturated drift velocities, the

¶ E-mail: P.Sellin@surrey.ac.uk

drift velocity v is related to drift mobility μ by the normal expression $v = \mu E$ such that drift length has the form

$$\lambda = \mu \tau E. \quad (2)$$

In the case of ion beam irradiation with 2 MeV protons, tha range of the ion is typically 50 μm. Consequently the electron hole pairs are generated in a shallow region very close to the irradiated contact and the resulting induced charge signal is predominantly due to the drift of a single carrier polarity. Consequently IBIC imaging is used to produce high resolution maps of either electron or hole CCE, depending on irradiation of the device cathode or anode, respectively.

The mean carrier drift length increases as an exponential function of the applied bias voltage, as described by the Hecht equation [9], which describes CCE as a function of the interaction depth x of the radiation from the cathode:

$$\varepsilon(x) = \frac{Q(x)}{N_0 q} = \frac{\lambda_h}{d}\left(1 - \exp\left(\frac{-x}{\lambda_h}\right)\right) + \frac{\lambda_e}{d}\left(1 - \exp\left(\frac{x-d}{\lambda_e}\right)\right) \quad (3)$$

and where the electric field is assumed constant as a function of depth.

For the condition that $x \ll d$ equation (3) can be simplified to the „single carrier“ case, where the CCE is given by

$$\varepsilon \approx \frac{\mu \tau V}{d^2}\left(1 - \exp\left(\frac{-d^2}{\mu \tau V}\right)\right) \quad (4)$$

and V is the applied bias. By applying equation (4) on a pixel-by-pixel basis to a sequence of IBIC maps acquired at increasing bias voltage, a quantitative map of either electron or hole $\mu\tau$ can be generated [10].

In time-resolved digital IBIC each individual preamplifier output pulse is digitized using a high speed waveform digitizer, and an appropriate software algorithm is applied to study the time evolution of each pulse. Typically the 10–90% risetime of the preamplifier pulse is measured and hence the carrier drift time τ_{dr} is calculated. This ion beam implementation of the well known „time of flight“ (TOF) technique is closely related to the conventional laser-induced TOF based on analysis of current transients [11–13]. The method requires that the field strength is uniform as a function of depth throughout the device in order to extract realistic drift mobility values.

In this way the drift mobility μ for either electrons or holes can be calculated from the carrier drift time measured using alpha or proton irradiation of the cathode, or anode, respectively. In the case of significant trapping where the mean drift length of the carriers is less than the device thickness ($\lambda < d$) the charge collection efficiency ε is used to estimate the actual drift distance, hence

$$\mu \approx \frac{d^2 \varepsilon}{\tau_{DR} V}. \quad (5)$$

3. Experimental System

IBIC experiments were carried out on several high quality semi-insulating CdTe samples supplied by Eurorad (France). The CdTe samples were doped with chlorine to achieve high resistivity ($\rho > 10^9\ \Omega \cdot$ cm). The devices used electroless metal contacts which gave ohmic-type behaviour with regard to the $I-V$ characteristics. Each device was mounted on a ceramic substrate, with a wire connection to the „top“ surface and a conducting adhesive forming a „rear“ connection to a gold track on the ceramic substrate. In all configurations, the bias voltage was supplied to the top contact via an Ortec 142A preamplifier, with the rear contact connected to ground.

The IBIC measurements were carried out at the nuclear micro-beam facility at the University of Surrey, using the University's High Voltage 2MV Tandetron accelerator [14] using 2 MeV proton beams. The IBIC facility is made up of focusing optics and beam scanning controls supplied by Oxford Microbeams Ltd. The beam was focused to a $< 4\,\mu$m diameter spot and raster-scanned across the surface of the CdTe device, using several scanning areas varying from 2.5×2.5 mm, to $200 \times 200\,\mu$m.

Operation of the IBIC data acquisition system is in two modes, either in an „analogue“ mode or using a time-resolved „digital“ system. For the conventional analogue mode [15], the output pulses from the 142A preamplifier are passed through a shaping amplifier and the induced charge signal amplitude is acquired at each pixel position using a multichannel analyser. The resulting high resolution maps of mean charge signal amplitude are directly related to the mean carrier drift length λ. A precision pulser is used with a known test capacitance to calibrate the system, by which the signal amplitude is calibrated in terms of energy deposited in CdTe (using an electron-hole pair creation energy $W = 4.4$ eV/ehp) and hence into CCE.

Time-resolved digital IBIC has also been implemented at the Surrey microbeam line, which is described in more detail in reference [16]. Fig. 1 shows a schematic of the most recent implementation of the digital IBIC system, which uses an 8-bit 1 GS/s PCI-based waveform digitiser card (Acqiris, Geneva) to capture individual pulses from the Ortec preamplifier. A second 12-bit 100 MS/s digitiser card

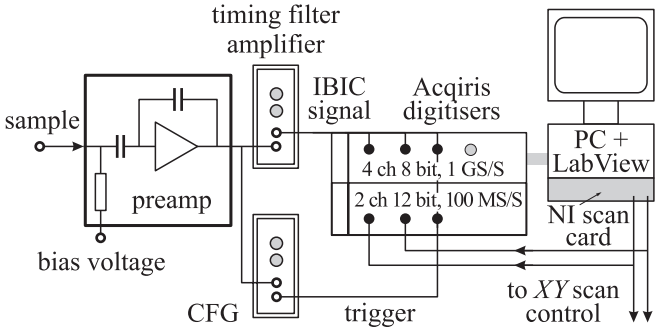

Figure 1. Schematic showing the digital IBIC data acquisition and control system.

is strobed with a common trigger signal, and captures the beam position from the X, Y beam control signals. Dedicated Labview software is used to apply digital pulse shape analysis algorithms to each pulse and so generate either signal amplitude or risetime spectra for each pixel. Digital IBIC maps of charge drift time can be generated for either electrons or holes, depending on the bias voltage polarity, which can be scaled into maps of drift mobility using equation (5).

4. Results and Discussion

4.1. Signal amplitude maps

Fig. 2, *a* shows an IBIC image acquired from a 9 mm thick CdTe sample which shows a region of a pixellated electrode structure, acquired with an applied bias of-150V. The pixel pitch in this device is 2.4 mm. The resulting map is generated by electron drift through the sample. The scan size, measuring an area of 1.8×1.8 mm, shows the corners of 4 pixels, plus the exposed inter-pixel gap where no charge is collected. The map is generated from 770.000 events using the integrated number of counts in each pulse height spectrum, which is typically 10–15 events per pixel. The data show a very uniform response from the majority of the device, with a region of poor performance in the top left quadrant of the map, which is associated with de-lamination of the metal contact in this region. A vertical projection through the map is also shown in Fig. 2, *b*, clearly indicating the lack of counts in the inter-pixel region, and in the circular feature in the top-right corner of the image. The statistical noise, due to the relatively small number of counts in each pixel is evident in both the map and the projection plot.

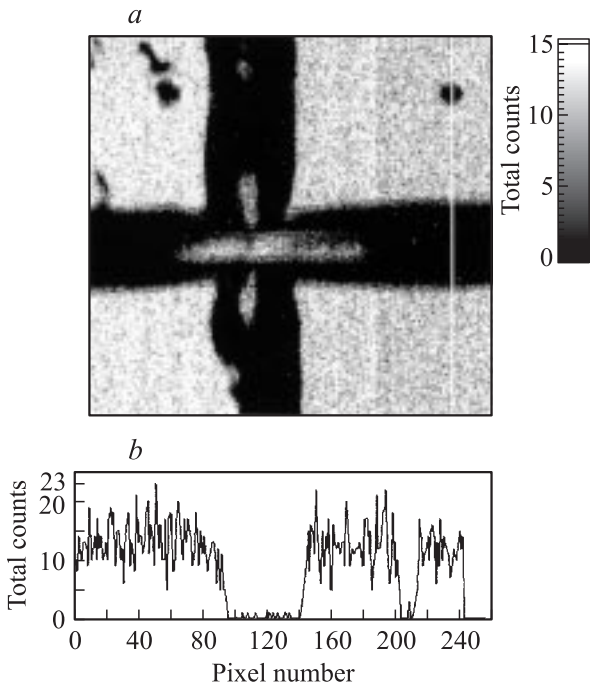

Figure 2. *a* — IBIC map from a pixellated CdTe device, plotting the total number of counts recorded at each pixel; *b* — a vertical projection at column $X = 230$. The applied bias was -150 V, with 770 K events recorded in the total data file.

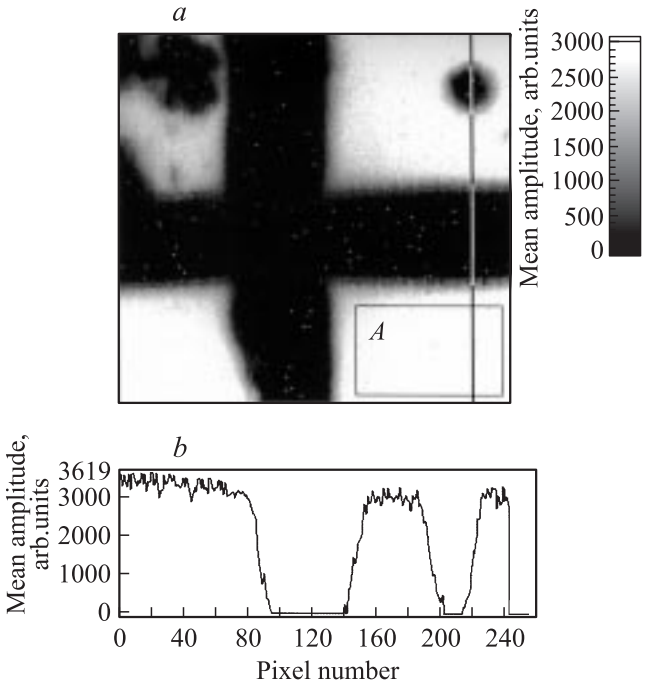

Figure 3. The same data file as Figure 2: *a* — with the IBIC map re-calculated in terms of mean pulse amplitude (arb. units); *b* — a vertical projection at column $X = 230$.

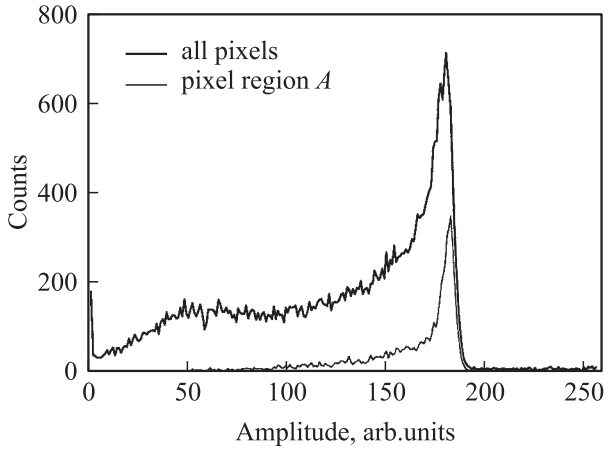

Figure 4. The pulse height spectrum acquired from the previous data; plotted from the whole map, and only from region A indicated in Fig. 3.

The use of a more sophisticated processing algorithm applied to the same data file is shown in Fig. 3, *a*. In this case the algorithm calculates the mean energy of all events occurring at each pixel, and the image therefore shows the average amplitude, or energy, per pixel. By appropriate normalization this data can be presented as charge collection efficiency ε or as mean carrier drift length λ. Fig. 4 shows the corresponding pulse height spectrum acquired from all pixels in the map, and from a limited region of uniform response (indicated „*A*“ in Fig 3, *a*).

The average amplitude map clearly shows a significant reduction in statistical noise compared to that of Fig. 2, which is also seen in the corresponding projection shown in Fig. 3, *b*. Clearly shown in the projected plot is the effect of reduced charge drift length at the edges of the electrodes. This reduction in drift length is directly caused by the reduced electric field strength close to the edges of the electrode which causes electron trapping. Comparison with Fig. 2 shows that the electric field extends for several hundred micrometers beyond the edge of the metal electrodes, although at a reduced field strength.

Figs 2 and 3 show a circular feature, approximately 100 μm in diameter, in the top right of the image. This is most likely caused by an extended defect in the bulk such as a tellurium inclusion which acts as an extended trapping centre. In general the CdTe:Cl material measured in this study, which was obtained from the central region of the grown wafer, was very free of this type of extended defect.

4.2. Hecht maps and $\mu\tau$ product

In a separate experiment 2.05 MeV protons were used to image electron transport in a second sample, which was a large area pixellated CdTe device with a thickness of 1.2 mm. Previous measurements of drift mobility on this sample ($\mu_e = 880\,\text{cm}^2/\text{Vs}$ and $\mu_h = 90\,\text{cm}^2/Vs$) [17–18] confirmed the good charge transport properties of this device. Fig. 5 shows the pulse height spectra obtained from this device as a function of bias voltage, with the protons incident on the cathode. The high quality of this material can be seen from the narrow resolution of the proton peaks, and the low bias voltage which is required to obtain a high charge collection efficiency. A Hecht fit to this data, using equation (4), gives $\mu\tau_e = 5.3 \cdot 10^{-3}\,\text{cm}^2/\text{V}$ for this device.

A sequence of identical IBIC scans, calibrated into charge collection efficiency, were acquired from this sample at bias voltages of -7, -14, -21, -28 and -34 V. An example image acquired at -34 V is shown in Fig. 6, *a* which shows the response of a single pixel with a scan size of 2×2 mm. The pixel region shows a generally highly uniform response with a CCE close to 100%. The edges of the pixel appear around the limits of the image, as regions of severely reduced response. Fig. 6, *b* shows the vertical projection at the indicated column.

An unexpected horizontal region of poor response is clearly visible running across the centre of the map in Fig. 6, *a*. This line feature, in which the CCE drops to $\sim 40\%$, continues into adjacent pixels on either side of the map. No visible scratches or similar surface features are observed on the sample, and this feature is consistent with a grain boundary in the bulk of the CdTe material.

Using the sequence of IBIC images at increasing bias voltages, a Hecht map of $\mu\tau_e$ was generated as shown in Fig. 7. The calculated $\mu\tau_e$ values are only valid for the region of the device covered by the electrode, where the electric field strength is constant. The $\mu\tau$ map provides a

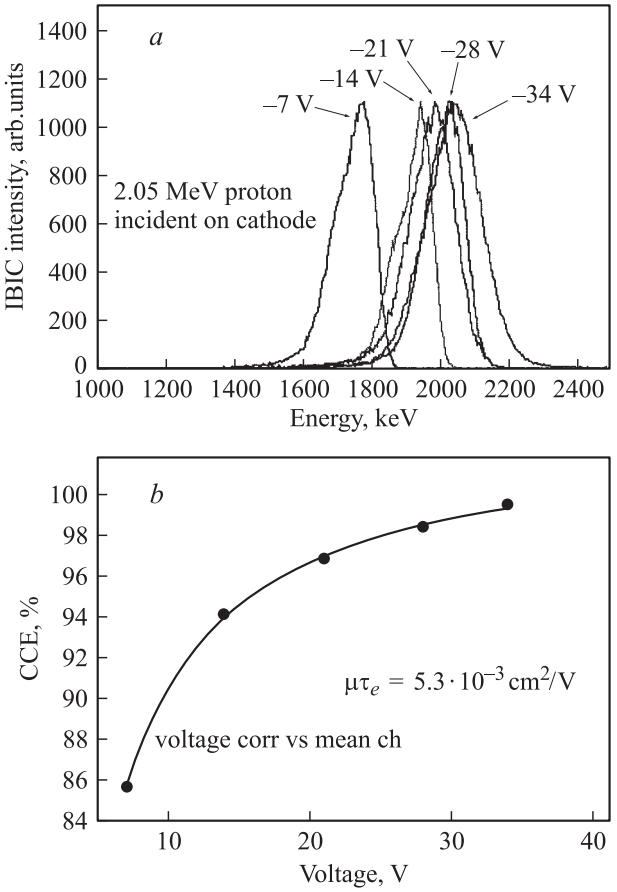

Figure 5. *a* — IBIC pulse height spectra obtained with 2.05 MeV protons, due to electron transport; *b* — plot of electron mean charge collection efficiency *vs* bias voltage, fitted to the single-carrier Hecht equation.

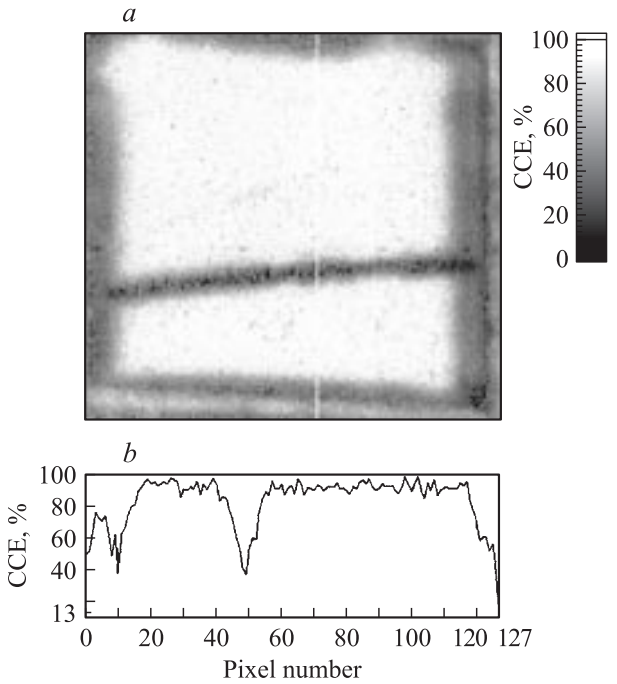

Figure 6. *a* — electron CCE map from a single pixel region, acquired at $V = -40$ V; *b* — vertical projection at the indicated line.

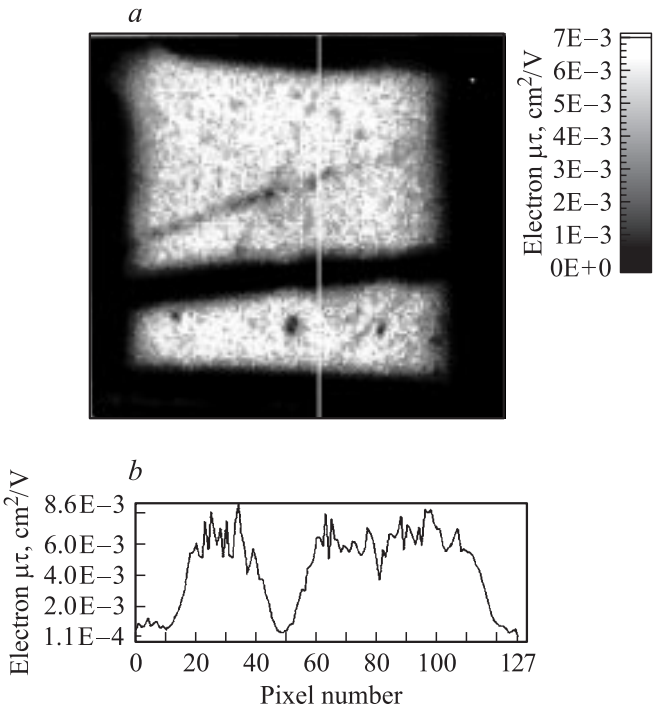

Figure 7. *a* — electron $\mu\tau$ map produced from the same data set as Fig. 6; *b* — vertical projection at the indicated line.

powerful quantitative measure to assess variations in charge transport across the device, and tends to bring out greater contrast of weak features compared to a single CCE map. This is evidenced by the weak diagonal line and the small circular regions of reduced $\mu\tau_e$ visible in Fig. 7.

4.3. Digital IBIC time-of-flight maps

The Surrey IBIC system provides simultaneous acquisition of both analogue and digital data sets during a single experiment. Examples of typical pulse shapes acquired from a 6 mm thick sample are shown in Figs 8 and 9. These demonstrate the use of a software FFT filter to remove high frequency noise from single pulses. Fig. 8 shows a typical electron pulse acquired at a voltage of -150 V with a 10–90% risetime of ~ 500 ns. The effect of software filtering is to remove the high frequency noise in the trace without distorting the risetime shape.

At very low bias voltages the analysis of pulse shapes becomes more complex, with a temperature dependent slow component often visible caused by thermal emission of trapped charge. In such cases the simple analysis of the pulse risetime in terms of drift mobility is no longer possible. Fig. 9 shows an axample of this type of pulse, where the risetime extends to $> 20\,\mu$s. Analysis of the slow component as a function of temperature can be used to probe trap activation energies, and this technique has recently been applied to the investigation of deep levels in synthetic diamond [19].

An example of time-resolved analysis from digital IBIC data is shown in Fig. 10, *a*, acquired simultaneously with that of Fig. 7 at a bias of -34 V. The 20–90% rise time of the pulse shapes is measured from the digital IBIC data, and re-calculated to show the mean electron drift time across the sample. The data show good uniformity of drift times in the central region under the electrode, as shown by the horizontal projection shown in Fig. 10, *b*. The average electron drift time in this device is 330 ns, which corresponds to an electron drift mobility of approximately 1200 cm^2/Vs. At the edges of the electrode a longer drift time is observed, which increases to 1 μs due to the reduced field strength in these regions.

Similar data is presented in Fig. 11, which shows a map of electron drift time from the 9 mm thick pixellated sample. In this data, at a bias voltage of -150 V, the high quality regions of the device show a mean drift time of 4 μs. The region around the circular feature in the upper right

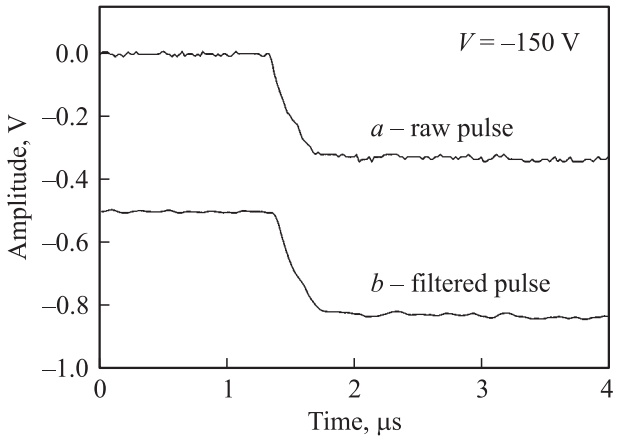

Figure 8. Example electron preamplifier pulse acquired during time-resolved IBIC from CdTe. This „fast“ pulse is at a bias voltage of -150 V, with a sample thickness of 6 mm. *a* — a single pulse without averaging; *b* — the same pulse after application of a high frequency software filter.

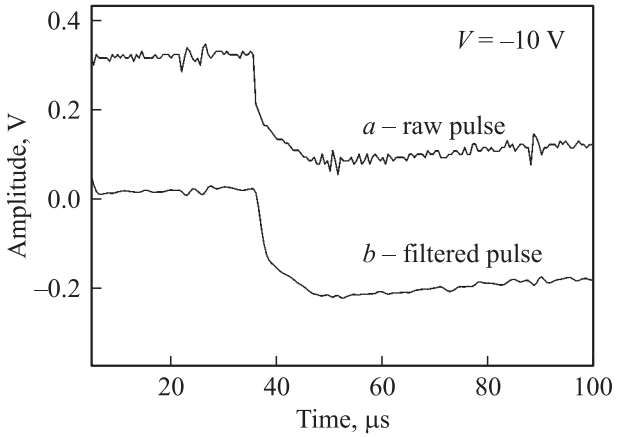

Figure 9. Example „slow“ electron preamplifier pulse acquired at a bias voltage of -10 V, showing a delayed slow component to the pulse shape. *a* — a single pulse without averaging; *b* — the same pulse after application of a high frequency software filter.

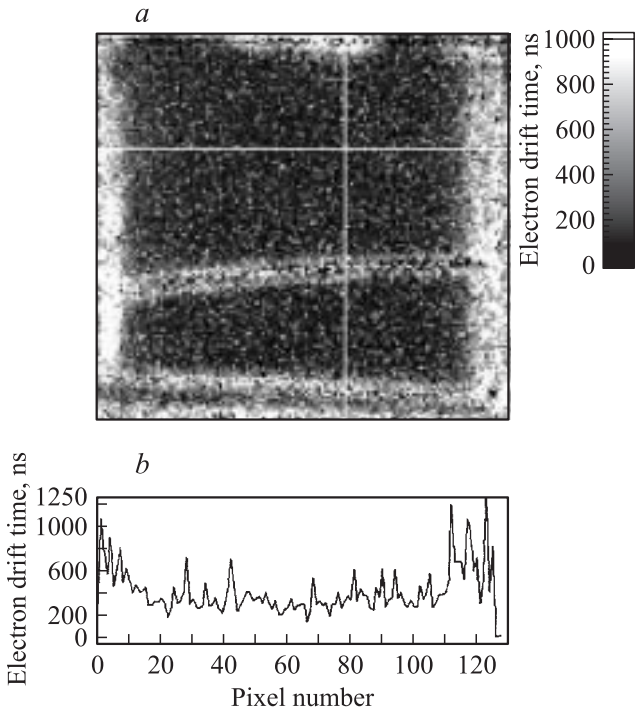

Figure 10. *a* — map of electron drift time for the same data set as Fig. 6, acquired at -50 V; *b* — horizontal projection at the indicated line.

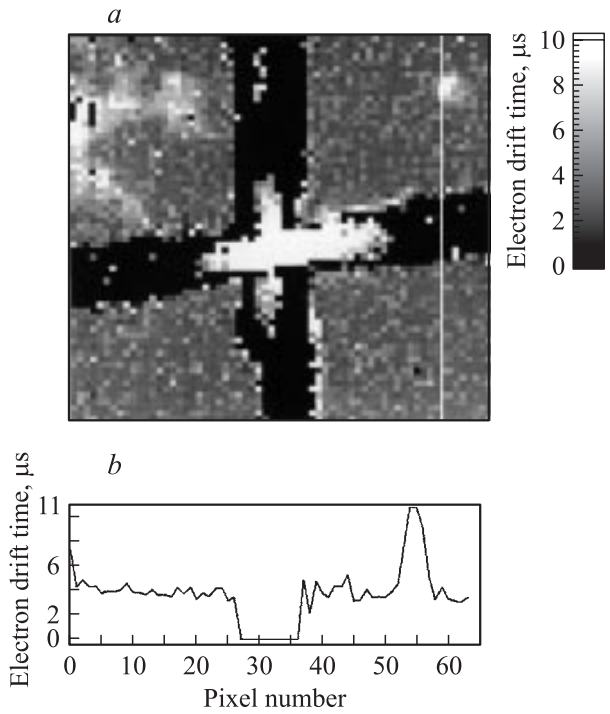

Figure 11. *a* — IBIC TOF maps showing electron drift time in a 9 mm thick pixellated CdTe device at a bias of -150 V; *b* — vertical projection at the indicated line.

quadrant shows a longer drift time of 11 μs, which suggests a reduced field strength in this region, and emphasizes the relatively long electron lifetime in the material.

5. Conclusion

High resolution quantitative mapping of charge transport in CdTe has been performed using the IBIC technique, which has demonstrated the excellent uniformity of electron and hole drift length of CdTe : Cl material grown by THM. Hecht maps show electron $\mu\tau$ values of $> 5 \cdot 10^{-3}$ cm^2/Vs which is consistent with previous reports. IBIC can also be used to investigate the device performance of CdTe radiation detectors, including the region of reduced electric field strength at the electrode edges, and the role of tellurium inclusions in degrading carrier transport. Time-resolved IBIC is used to perform time of flight mapping of carrier drift mobility, which also demonstrates the excellent uniformity of carrier lifetime and mobility in this material.

The authors gratefully acknowledge Eurorad for the supply of the CdTe samples. This project was partly supported by the European Union Framework 5 „Nucam“ project, and by the EPSRC Instrument Development grant reference GR/R34486/01.

References

[1] P.J. Sellin. Nucl. Instrum. Methods A **513** (1–2), 332 (2003); A. Owens, A. Peacock. Nucl. Insturm. Methods A **531** (1–2), 18 (2004); P.J. Sellin. Nucl. Instrum. Methods A **563** (1), 1 (2006).
[2] S. Rath, P.J. Sellin, M.B.H. Breese, H. Herman, L.C. Alves, A.H. Holland. Nucl. Instrum. Methods A **512**, 427 (2003).
[3] M. Ayoub, M. Hage-Ali, A. Zumbiehl, R. Regal, J.M. Koebel, C. Rit, P. Fougeres, P. Siffert. IEEE Trans. Nucl. Sci. **49** (4; Pt. 1), 1954 (2002).
[4] J. Shen, D.K. Aidun, L. Regel, W.R. Wilcox. Materials Sci. Engineering **16** (1/3), 182 (1993).
[5] N.V. Sochinskii, M.D. Serrano, E. Dieguez, F. Agullo-Rueda. J. Appl. Phys. **77** (6), 2806 (1995).
[6] M. Amman, J.S. Lee, P.N. Luke. J. Appl. Phys. **92** (6), 3198 (2002).
[7] K. Hecht. Z. Phys. **77**, 235 (1932).
[8] A. Lohstroh, P.J. Sellin, A. Simon. J. Physics Condensed Matter **16** (2), S67 (2004).
[9] L. Verger, N. Baffert, M. Rosaz, J. Rustique. Nucl. Instrum. Methods A **380**, 121 (1996); K. Suzuki, A. Iwata, S. Seto, T. Sawada, K. Imai. J. Cryst. Growth **214–215**, 909 (2000); K. Suzuki, S. Seto, T. Sawada, K. Imai. IEEE Trans. Nucl. Sci. **49** (3; Pt. 2), 1287 (2002).
[10] A. Simon, C. Jeynes, R.P. Webb, R. Finnis, Z. Tabatabaian, P.J. Sellin, M.B. Breese, D.F. Fellows, R. van den Broek, R.M. Gwilliam. Nucl. Instrum. Methods B **219–220**, 405 (2004).
[11] M.B. Breese, D.N. Jamieson, P.J.C. King. *Materials analysis using a nuclear microprobe*. (Wiley, New York, 1996).
[12] P.J. Sellin, A. Lohstroh, A. Simon, M.B. Breese. Nucl. Instrum. Methods A **521** (2–3), 600 (2004).
[13] A.W. Davies, A. Lohstroh, M.E.Özsan, P.J. Sellin. Nucl. Instrum. Methods A **546** (1–2), 192 (2005); P.J. Sellin, A.W. Davies, A. Lohstroh, M.E. Özsan, J. Parkin. IEEE Trans. Nucl. Sci. **52** (2), 3074 (2005).
[14] S.Wang, P. Sellin, A. Lohstroh. Appl. Phys. Lett. **88** (2), 023 501 (2006).

Редактор Л.В. Беляков